Effect of tilted magnetic field on the magnetosubbands and conductance of bi-layer quantum wire

T. Chwiej*
AGH University of Science and Technology, al. A. Mickiewicza 30, 30-059 Cracow, Poland

The single electron magnetotransport in a vertical bi-layer semiconductor nanowire made of InAlAs/InGaAs and AlGaAs/GaAs heterostructure is theoretically studied. The magnetic field is directed perpendicularily to the main (transport) axis of the quantum wire and both non-zero components of magnetic field, that is the transverse and the vertical ones, allow to change the magnitude of intra-layer and inter-layer subbands mixing, respectively. We analyze in detail the changes introduced to energy dispersion relation E(k) by strong titled magnetic field up to several teslas for a symmetric and an asymmetric confining potential in the growth direction. These calculated energy dispersion relations are thereafter used to show that the value of conductance of bi-layer nanowire may jump as well as drop by few conductance quanta when the Fermi energy is changed what in conjunction with spin Zeeman effect may give a moderately spin polarized current.

PACS numbers: 72.25.Dc,73.21.Hb
Keywords: quantum wire, ballistic transport, spin polarized transport

I. INTRODUCTION

The electron transport properties of a nanosystem consisting of two quantum wires being placed close to each other depends largely on the magnitude of their tunnel coupling.[1–5] For strong and moderate coupling strength the electron's wave functions originating from separate wires can hybridize and the magnitude of hybridization depends naturally on the energy splitting of the electron's subbands and the electron's wave functions overlap. The last two quantities are particularily sensitive to the strength of magnetic field and its direction.[6,7] If magnetic field is directed along the main axis of a coupled wires system, it squeezes the electron's wave functions what leads to their stronger localization within particular nanowire and in consequence it weakens the effect of subbands hybridization.[7,8] However, if direction of magnetic field is set perpendicularily to the axis of a nanosystem, then the Lorentz force pushes the electrons to the edges of the nanowires. The wave functions being pushed to the central barrier separating the wires can be in such case easily mixed. Such inter-wire subbands mixing by perpendicular magnetic field transforms the crossings of hybridized subbands in the energy dispersion relation E(k) into anticrossings.[3,9] Inside an anticrossing a pseudogap is formed what means that the conductance of two coupled nanowires is lowered when the Fermi energy level is raised and enters this region. Qualitatively mechanism of the pseudogaps formation in E(k) spectrum in magnetic field is the same for two laterally or vertically coupled nanowires systems. However in practical applications a nanosystem built of two vertically coupled wires has advantage over a system with two wires aligned laterally since: i) it allows to tune the Fermi energy in particular wire independently of its value in the second one by means of the top, bottom and side gates[5,10–13] and, ii) each of the three components of magnetic field modifies in a different manner the conductance of a nanosystem[4,14] giving thus an opportunity to control over a single subband.[14]

In this paper, we theoretically analyze the effect of tilted magnetic field on a single electron transport in a bi-layer quantum wire made of a double inverted heterostructure like InAlAs/InGaAs and AlGaAs/GaAs. We assume the electron current flows in the wire (along x axis) without scattering i.e. the electron transport is ballistic, layers are vertically aligned in z (growth) direction one over another and the surrounding confining potential is formed by the rectangular barriers. Direction of magnetic field is perpendicular to the wire axis, that is only its vertical (B_z) and transverse (B_y) components have non-zero values and both can be changed independently with precision.[15] Such approach give us an ability to tune an interlayer and intralayer modes coupling by changing B_y and B_z, respectively. First, we discuss how the simultaneous mixing of the vertical and the transverse eigenstates for the assumed double-well confining potential modifies the energy dispersion relation $E(k)$ of bi-layer nanowire. Next the oscillating behaviour of magnetosubbands in vicinity of $k = 0$ is considered in context of the conductance variations as function of Fermi energy. We show that for a nanosystem working in a ballistic regime these oscillations give contribution to the wire conductance which may jump as well as drop by few conductance quanta when Fermi energy level is successively raised or lowered between two neighbouring pseudogaps. In the last part of this paper we discuss a possibility of application of bilayer quantum wire as a source of partly spin polarized current for moderate Fermi energies.

Paper is organized as follows. In Sec.II we present theoretical model used in calculations, properties of magnetosubbands for tilted magnetic field are discussed in Sec.III while in Sec.IV we present the potential application of pseudogaps appearing in energy spectrum for partial spin polarization of conductance. We end up with conclusions given in Sec.V.

II. THEORETICAL MODEL

The confining potential in a conventional semiconductor quantum wire can be formed electrostatically by gating the 2DEG[13], etching of nano-grooves[5] on the layered nanostructure that holds 2DEG few tens of nanometers beneath the surface or by cleaved-edge overgrowth.[16] In all cases the 2DEG is formed within a square well created by double inverted heterojunction.[5] The first three methods give soft lateral confining potential which was widely used in theoretical works before[17,18] while the last one generates rectangular confinement that we have adopted for this work. We consider a quantum wire in which the electrons can move freely along x axis but their motion in y-z plane is quantized due to the rectangle shapes of external barriers. The quantum well is defined for $y \in [-a, a]$ and $z \in [-b, b]$ with high confining potential outside this region. Throughout this paper we use $a = 50$ nm and $b = 15$ nm. For simplicity we assume the barrier surrounding the wire is infinite while the confining potential inside the channel depends only on position in the growth direction (z-axis) i.e. $V(\boldsymbol{r}) = V(z)$. We model the confining potential by formula:

$$V(z) = V_{max}[sin\left((1 + z/b)\pi/2\right) + \alpha sin\left(\pi(1 + z/b)\right)] \quad (1)$$

which describes the potential with maximum localized in a central region of original well [non-zero parameter α breaks the symmetry in $V(z)$]. Such potential is formed within a wide quantum well when one delta doping layer is placed below and another one above the well. Then, the positively ionized dopants effectively lower the confining potential near both edges of the well giving thus a bi-layer coupled system within a single nanowire.[7,19] Depth of an upper well, or in other words the value of parameter α, can be adjusted by changing the voltage applied to the central top gate[8] which may cover the whole structure[20] or to the top split gate.[7]

An example of a such confining potential is showed in Fig.1(a). A bi-layer system can be also formed by stacking two quantum wires one above the other during the epitaxial growth with very narrow tunnel barrier separating them.[5,12,14] Since all effects, we investigate here, depend mainly on the energy difference between two lowest eigenstates of vertical quantization, an actual shape of vertical confinement is of little importance and the results presented below are representative for both types of confinements. Both layers, the upper and the lower one are pierced by magnetic field which has $B_x = 0$ whereas the values of two other components can be freely changed. Since magnetic field lifts spin degeneracy, we limit our considerations to subbands with spins set parallel to magnetic field until otherwise stated. The energies for subbands with antiparallel spins can be simply obtaned by adding spin-Zeeman splitting energy $\Delta E_Z = g\mu_B B$. In calculations we use a non-symmetric vector potential $\boldsymbol{A} = [zB_y - yB_z, 0, 0]$ for which the single electron Hamiltonian reads:

$$H = -\frac{\hbar^2}{2m^*}\nabla^2 + \frac{Iq\hbar}{m^*}A_x\frac{\partial}{\partial x} + \frac{q^2}{2m^*}A_x^2 \quad (2)$$

where: I is an imagnary unit, $q = -e$ is an electron's charge and m^* is its effective mass ($m^* = 0.067$ for GaAs and $m^* = 0.04$ for InGaAs). The eigenstates of Hamiltonian given by Eq. 2) can be expressed as the linear combination of products of the plane waves for x direction and the eigenstates for the transverse (y-axis) and vertical (z-axis) directions. We define the electron's wave function for p-th subband and the wave vector k as follows:

$$\Psi_{p,k}(\boldsymbol{r}) = e^{Ikx}\sum_{m=1}^{M}\sum_{i=1}^{N} c_{m,i}^{(p)} \cdot f_m(z) \cdot \varphi_i(y) \quad (3)$$

In Eq. 3, $f_m(z)$ and $\varphi_i(y)$ are the basis functions for quantization in z and y directions, respectively. Due to infinite barriers surrounding the quantum wire, the normalized basis functions for y direction are simply:

$$\varphi_i(y) = sin\left[i \cdot \pi(1 + y/a)/2\right]/\sqrt{a}, \quad i = 1, 2, \ldots, N \quad (4)$$

The basis functions $f_m(z)$ have been found by solving the eigenproblem for z direction i.e. $\widehat{h}_z f_m = E_m^z f_m$ with Hamiltonian $h_z = -(\hbar^2/2/m^*)\partial^2/\partial z^2 + V(z)$. The coefficients of linear combination $c_{m,i}^{(p)}$ appearing in Eq. 3 are real numbers which are strictly 0 or 1 when magnetic mixing is absent ($B_y = B_z = 0$) otherwise they fulfill condition $|c_{m,i}^{(p)}| \leq 1$.

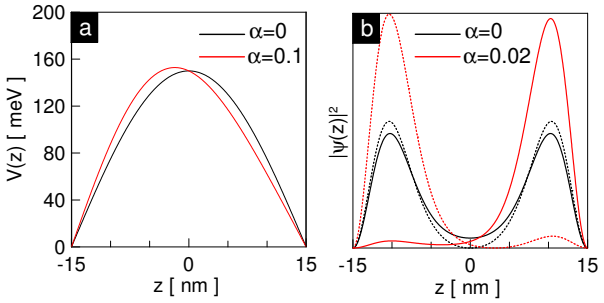

FIG. 1: (Color online) a) Cross-section of a confining potential in z direction for $\alpha = 0$ and $\alpha = 0.1$ (left and right axes are the infinite barriers). b) Probability density distributions of two lowest eigenstates of vertical quantization for symmetric ($\alpha = 0$ - black color) and nonsymmetric ($\alpha = 0.02$ - red color) confining potentials. Continous curves stand for the ground state while dashed lines for the first excited one. In (a) and (b) $V_{max} = 150$ meV.

The maximum in the confining potential divides the original well into two narrower tunnel-coupled wells which for $\alpha = 0$ have the same eigenenergies. Figure 1(b) shows the probability densities for the ground $[f_1(z)]$ and the first excited $[f_2(z)]$ eigenstates of Hamiltonian h_z. We notice that for large amplitude of $V(z)$ [see Eq.1],

the densities are localized mainly in two narrower wells but mutually overlap to some extent. Since energy difference for these eigenstates $[\Delta E_{21}^{(z)} = E_2^{(z)} - E_1^{(z)}]$ is small, even a small distortion in the confinement [$\alpha = 0.02$ in Figs.1(b)] can significantly mix them what may result in their spatial separation [red curves in Fig.1(b)]. Therefore, these two thin wells form two transport layers and the nanowire becomes in fact a bi-layer system. To get deeper insight into nature of this process, we calculate $\Delta E_{21}^{(z)}$ as function of V_{max}. This dependency is showed in Fig.2(a). In spite of $\alpha's$ value, $\Delta E_{21}^{(z)}$ decreases if V_{max} grows but the lowest $\Delta E_{21}^{(z)}$ we get always for $\alpha = 0$. For $\alpha > 0$, the ground state is localized in the upper well what minimizes its energy while the first excited one occupies the lower well because of orthogonality constrictions but for the price of its increased energy.[20] Due to a large energy separation of higher eigenstates $f_m(z)$ $(m = 3, 4, \ldots)$ we have neglected them in calculations and use $M = 2$ in Eq.3 while the number of transverse modes $\varphi_i(y)$ was limited to $N = 30$.

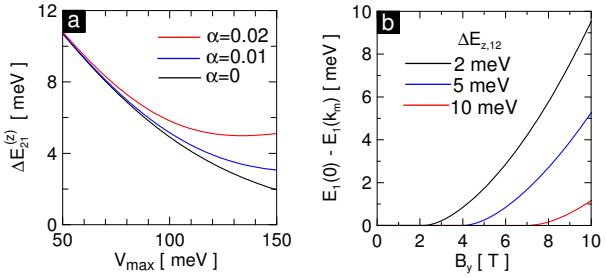

FIG. 2: (Color online) a) Energy difference $\Delta E_{21}^{(z)}$ between the first and second eigenstates for vertical direction in dependence on V_{max} and for different values of α. b) An energy difference between maximum ($k = 0$) and minimum (k_m) of lowest subband in dependence on B_y. In (b) results were obtained for $V_{max} = 150$ meV and $\alpha = 0$.

Having the wave functions defined by Eq.3, we may used them to transform an original Hamiltonian given by Eq.2 to much simpler algebraic form. For this purpose, we first eliminate x variable from Hamiltonian H by averaging it over this variable: $H_{y,z} = \langle e^{-Ikx}|H|e^{Ikx}\rangle$. Reduced Hamiltonian then reads:

$$H_{yz} = -\frac{\hbar^2}{2m^*}\left(\nabla_{y,z}^2 + k^2\right) - \frac{q\hbar k}{m^*}A_x + \frac{q^2}{2m^*}A_x^2 + V(z) \quad (5)$$

Next, we calculate $H_z = \langle\varphi_i(y)|H_{yz}|\varphi_j(y)\rangle$ and thereafter $H^{eff} = \langle f_l(z)|H_z|f_m(z)\rangle$. The effective Hamiltonian has the following form:

$$H^{eff} = H_0^{eff} + H_1^{eff} + H_2^{eff} + H_3^{eff} \quad (6)$$

$$H_0^{eff} = \left(\frac{\hbar^2\gamma_j^2}{2m^*}\delta_{i,j} + E_m^z\delta_{i,j} + \frac{1}{2m^*}Y_{i,j}^{(2)}\right)\delta_{l,m} \quad (7)$$

$$H_1^{eff} = \frac{m^*\omega_y^2}{2}Z_{l,m}^{(2)}\delta_{i,j} \quad (8)$$

$$H_2^{eff} = -\omega_y\hbar k\delta_{i,j}Z_{l,m}^{(1)} \quad (9)$$

$$H_3^{eff} = -m^*\omega_y\omega_z Y_{i,j}^{(1)}Z_{l,m}^{(1)} \quad (10)$$

In above array of equations we have assumed: $\gamma_j = j\pi/2/a$, $j = 1, 2, \ldots, N$; $\omega_y = qB_y/m^*$, $\omega_z = qB_z/m^*$; $Z_{l,m}^{(1)} = \langle f_l|z|f_m\rangle$; $Z_{l,m}^{(2)} = \langle f_l|z^2|f_m\rangle$; $Y_{i,j}^{(1)} = \langle\varphi_i|y|\varphi_j\rangle$; $Y_{i,j}^{(2)} = \langle\varphi_i|(m^*\omega_z y + \hbar k)^2|\varphi_j\rangle$; and $\delta_{i,j}$ is a Kronecker's delta. Indices (i, j) stand for transverse modes (defined in Eq.4) while pair of (l, m) mark the vertical ones. The effective Hamiltonian has matrix form which for only two-element basis $\{f_m(z)\}$ becomes 2×2 block matrix with real elements:

$$\boldsymbol{H}^{eff} = \begin{bmatrix} \boldsymbol{H_{11}} & \boldsymbol{H_{12}} \\ \boldsymbol{H_{21}} & \boldsymbol{H_{22}} \end{bmatrix} \quad (11)$$

Since all terms appearing in Eqs.7-10 are real, we immediately get condition $H_{21} = H_{12}$. The only term depending on $\delta_{l,m}$ is H_0^{eff} and therefore it contributes to diagonal submatrices H_{11} and H_{22} (their rank equals N that is the number of basis states φ_i). In consequence H_0^{eff} does not mix z-eigenstates. If confining potential V_z is symmetric ($\alpha = 0$) then the wave function $f_1(z)$ has even parity (ground or bounding state) while $f_2(z)$ has odd parity (first excited or antibonding state). Since the term $Z_{l,m}^{(2)}$ has itself even parity, the matrix elements H_1^{eff} give contributions only to diagonal submatrices, otherwise ($\alpha > 0$) they contribute also to off-diagonal submatrix H_{12}. On the other hand, term $Z_{l,m}^{(1)}$ has odd parity for $\alpha = 0$. It mixes vertical states f_1 and f_2 and in consequence gives contribution to H_{12} due to H_2^{eff} and H_3^{eff} terms. Notice, that for $\alpha > 0$ these Hamiltonians give contributions to diagonal matrices H_{11} and H_{22}.

III. RESULTS

A. Two-state model for $B_z = 0$

For $B_z = 0$ there is no mixing between basis states $\{\varphi_i(y)\}$ since the term $Y_{i,j}^{(1)}$ disappears in H^{eff} while term $Y_{i,j}^{(2)}$ reduces to $Y_{i,j}^{(2)} = \hbar^2k^2\delta_{i,j}$ due to $\omega_z = 0$ [see Eqs.7-10]. This gives us possibility to limit our considerations for a moment to the case with $N = 1$ keeping in mind that energy dispersion $E(k)$ for transverse modes φ_i with indcies $i > 2$ are strictly replicas of that with $i = 1$. Then, only diagonal elements of H^{eff} are shifted towards higher energy in the same manner. The two-state Hamiltonian now reads:

$$\boldsymbol{H}^{eff} = \begin{bmatrix} H_0^{eff}+H_1^{eff} & H_2^{eff} \\ H_2^{eff} & H_0^{eff}+H_1^{eff} \end{bmatrix} \tag{12}$$

$$= \begin{bmatrix} \frac{\hbar^2(\gamma_1^2+k^2)}{2m^*}+E_1^{(z)}+\frac{m^*\omega_y^2}{2}Z_{1,1}^{(2)} & -\omega_y\hbar k Z_{1,2}^{(2)} \\ -\omega_y\hbar k Z_{1,2}^{(2)} & \frac{\hbar^2(\gamma_1^2+k^2)}{2m^*}+E_2^{(z)}+\frac{m^*\omega_y^2}{2}Z_{2,2}^{(2)} \end{bmatrix} \tag{13}$$

Eigenvalues of $\boldsymbol{H}^{eff}$ can be written as:

$$E_{1,2} = \frac{\hbar^2k^2}{2m^*} + A_3 \pm \frac{|A_1|}{2}\sqrt{1+\left(\frac{A_2}{A_1}\right)^2 k^2} \tag{14}$$

where we have used following abbrievations: $A_1 = \left(E_2^{(z)}-E_1^{(z)}\right)+\frac{m^*\omega_y^2}{2}\left(Z_{2,2}^{(2)}-Z_{1,1}^{(2)}\right)$; $A_2 = 2\omega_y\hbar Z_{12}^{(1)}$; $A_3 = \frac{\hbar^2\gamma_i^2}{2m^*}+\left(E_1^{(z)}+E_2^{(z)}\right)/2+\frac{m^*\omega_y^2}{4}\left(Z_{1,1}^{(2)}+Z_{2,2}^{(2)}\right)$. Energy dispersion relation $E(k)$ for these two subbands are displayed in Fig.3(a) (black color). In first subband there are three extremums: two minimums separated by maximum localized at $k=0$. Localization of minimums can be found by imposing condition on dispersion relation $\partial E/\partial k|_{k=k_m}=0$ what gives:

$$k_m = \pm\sqrt{\left(\frac{m^*}{2\hbar^2}\right)^2 A_2^2 - \left(\frac{A_1}{A_2}\right)^2} \tag{15}$$

Value of k_m depends on A_1 and A_2 and therefore, for a fixed geometry and values of material parameters of nanowire, the non-zero value of k_m depends only on B_y due to requirement of non-negativity of expression in square root in Eq.15. Minimal value of B_y that gives $k_m>0$ can be estimated from the following formula:

$$B_y^{min} > \sqrt{\frac{2m^*}{q^2}\frac{\left(E_2^{(z)}-E_1^{(z)}\right)}{4\left(Z_{1,2}^{(1)}\right)^2-\left(Z_{2,2}^{(2)}-Z_{1,1}^{(2)}\right)}} \tag{16}$$

For $\alpha=0$, when energy difference $\Delta E_{21}^{(z)}$ is determinated by value of V_{max}, the increase of V_{max} decreases value of $\Delta E_{21}^{(z)}$ and consequently smaller B_y^{min} is needed for lateral minima to appear. Such dependence is displayed in Fig.2(b) which shows a difference between maximum and minimum of energy for first subband in function of B_y value. Simply, the lower $\Delta E_{21}^{(z)}$ is, the lower B_y is needed for this difference to have non-zero value. In close vicinity of $k=0$ the squared term in Eq.15 can be expanded in power series of k. Neglecting the terms with exponents greater than 3 which are small, we get the parabolic shape of energy dispersion:

$$E_{1,2}\,|_{k\to 0} = A_3 \pm \frac{|A_1|}{2} + k^2\left(\frac{\hbar^2}{2m^*} \pm \frac{1}{4}\frac{A_2^2}{|A_1|}\right) \tag{17}$$

where sign $+(-)$ corresponds to upper (lower) subband. For $k=0$, the energy difference between both subbands equals $|A_1|$ and depends on the sum of two differences: i) $\left(E_2^{(z)}-E_1^{(z)}\right)$ and, ii) $\left(Z_{2,2}^{(2)}-Z_{1,1}^{(2)}\right)$. Let us notice that, for increasing value of V_{max} both basis states for vertical direction i.e. $f_1(z)$ and $f_2(z)$ becomes degenerated [Fig.2(a)] with similar densities [Fig.1(b)]. For this reason, the energy difference between two lowest subbands gets smaller when V_{max} is increased for $k=0$. Appearance of two additional energy minimums

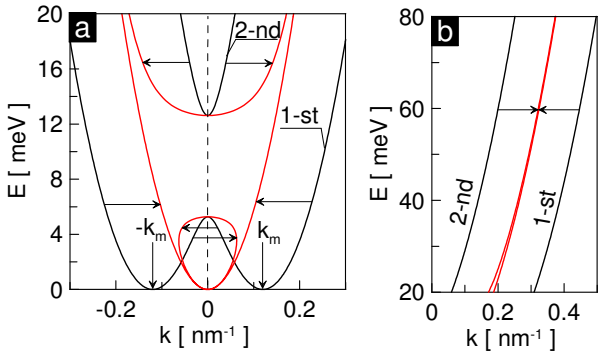

FIG. 3: (Color online) Energy dispersion relation in function of canonical wave vector k (black line) and kinetic wave vector k_{kin} (red line) for two lowest subbands. Figure (b) is continuation of (a) for higher energy and shows degeneracy of both subbands as function of kinetic wave vector k_{kin}. Horizontal arrows on (a) show directions of wave vector transformation $k\to k_{kin}$ while vertical ones mark energy minima in first subband. Parameters used in calculations: $B_y=10$ T, $B_z=0$, $\alpha=0$, $\Delta E_{21}^{(z)}=5$ meV. All energies are given with respect to a bottom of the lowest subband.

in magnetosubbands brings severe consequences for electron transport. If B_y is large enough to create energy minima then the kinetic wave vector $k_{kin}=\langle k+qA_x/\hbar\rangle$ becomes negative for $k\in(0,k_m)$. Similarly, due to symmetry of a confinig potential, for negative k in the range $k\in(-k_m,0)$, the effective wave vector becomes positive. Any oscillations in energy depending on canonical wave vector k produce thus negative energy dispersion relations. To study this problem in detail we have plotted the energies of two lowest subbands in function of k_{kin} in Fig.3 (red color). After transformation $k\to k_{kin}$, the dependence of electron's energy on k_{kin} becomes ambiguous for the first subband when k_{kin} is small. It consists of two curves: the closed loop surrounded by a parabolic

branch. The horizontal arrows in Fig.3 indicates directions of the wave vector's transformations. First, let us notice that for the closed loop, $k \in [-k_m, 0]$ transforms to $k_{kin} > 0$ and due to symmetry $k \in [0, k_m]$ transforms to $k_{kin} < 0$. Second remark concerns the scalability of k_{kin}. In Fig.3(a) we see that value of kinetic wave vector is compressed for the lower subband and expanded for the second one with respect to canonical wave vector value. And last, the two lowest subbands become degenerated for much larger Fermi energies what is showed in Fig.3(b). It means that electrons in both subbands move with the same group velocity $v_{gr} = \hbar k_{kin}/m^*$. This fact can be easily explained if energy dispersion relation given by Eq.17 will be expressed as function of k_{kin} instead of k. For this purpose, we first calculate an expectation value of kinetic wave vector for p-th subband:

$$\langle k_{kin}^{(p)} \rangle = k - \sum_{l=1}^{M} \sum_{m=1}^{M} c_{l,1}^{(p)} c_{m,1}^{(p)} \frac{m^* \omega_y}{\hbar} Z_{l,m}^{(1)} \qquad (18)$$

where coefficents $c_{l,1}^{(p)}$ and $c_{m,1}^{(p)}$ are components of two-element effective Hamiltonian ($p = 1, 2$) given by Eq.13. Using the components of two orthogonal eigenvectors, after some algebra we obtain a formula for the kinetic wave vectors:

$$\langle k_{kin} \rangle = k \left(1 \mp \frac{m^*}{2\hbar^2} \frac{A_2^2}{\sqrt{A_1^2 + A_2^2 k^2}} \right) \qquad (19)$$

where $(-)$ stands for first (lower) subband while $(+)$ for the second (upper) one. Assuming very large k value we may expand expression with square root leaving only the first term and then rearrange equation to get k: $k \approx k_{kin} \pm \frac{m^*}{2\hbar^2}|A_2|$. Substitution this approximate expression for k into Eq.14 gives:

$$E\left(k_{kin}^{(p)}\right) = \frac{\hbar^2}{2m^*}\left(k_{kin}^{(p)}\right)^2 + A_3 - \frac{m^*}{8\hbar^2}A_2^2 \qquad (20)$$

Now, it is easily to notice that if the kinetic wave vectors for the first and second subbands have the same value then these subbands are degenerated [Fig.3(b)].

B. Inter-layer subbands mixing for a non-symmetric confining potential

In this section we consider an effect of pure inter-layer subbands mixing ($B_z = 0$) on the energy dispersion relation for $\alpha > 0$ and on the conductance of a bi-layer nanowire. In Fig.4 we have plotted the low energy spectra calculated within our model for $\alpha = 0$ and $\alpha = 0.02$. If there is no in-plane magnetic field [first row in Fig.4], the vertical eigenmodes are not mixed and the symmetry of energy dispersion i.e. $E(k) = E(-k)$ is kept independently of $\alpha's$ value. For $\alpha = 0.02$ the energy branches of subsequent subbands are only shifted upwards on energy scale in comparison to the case with $\alpha = 0$. When

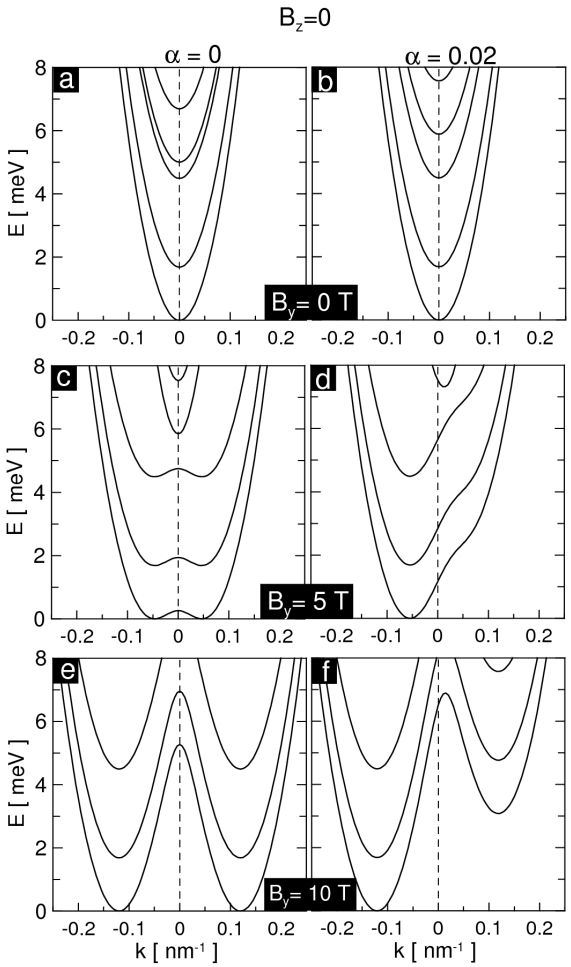

FIG. 4: (Color online) Energy dispersion relation for $\alpha = 0$ ($\Delta E_{21}^{(z)} = 5$ meV, left column) and $\alpha = 0.02$ ($\Delta E_{21}^{(z)} = 5.88$ meV, right column). All energies are given with respect to a bottom of the lowest subband.

value of B_y is increased to 5T [second row in Fig.4], then for $\alpha = 0$ the negative energy dispersion relation appears ($k_m > 0$) in the three lowest energy subbands which correspond to the ground, the first and the second excited states for y direction. However, the difference between the maximum and minimum of energy for each of these subbands is very small since it equals only 0.25 meV. If potential $V(z)$ becomes slightly nonsymmetric for $\alpha = 0.02$, it destroys the symmetry of subbands too. In such case, the upper quantum well is wider than the lower one what leads to a larger energy separation between the basis states $f_1(z)$ and $f_2(z)$ which for $\alpha = 0.02$ is $\Delta E_{21}^{(z)} = 5.88$meV. Although, this growth is not large, it is sufficient to suppress the negative energy dispersion relation for the moderate value of an in-plane magnetic field ($B_y = 5$T) since it is too small to overcome B_y^{min} defined in Eq.16. In this case, the electrons which have $k > 0$ and are localized in the lower layer due to an action of the magnetic force, have higher

energies than those with $k < 0$ [see localization of electron densities in Fig.1(b)] which move in a wider upper well. For this reason, the right parts of the energy spectra in Figs.4(d) and (f) are shifted upwards with respect to their left parts. Stronger magnetic field ($B_y = 10$ T) enhances the negative energy dispersion in relation to $\alpha = 0$ case. In Fig.4(e) we may notice that the difference between maximum and minimum of energy equals 5 meV for three lowest subbands and is much larger when compared to fraction of meV we have got for $B_y = 5$ T. Mixing of vertical subbands is now so strong that the negative dispersion relation of energy is reconstructed also for $\alpha = 0.02$ [cf. Figs.4(d) and (f)].

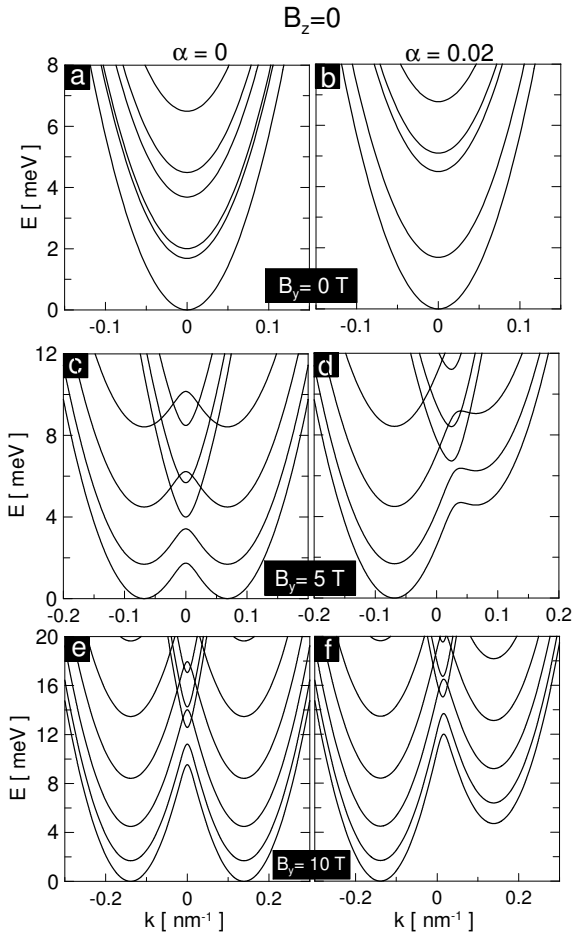

FIG. 5: (Color online) Energy dispersion relation for $\Delta E_{21}^{(z)} = 2$ meV (left column) and $\Delta E_{21}^{(z)} = 5.09$ meV (right column) and $B_z = 0$. Values of α are given on top of each columns. All energies are given with respect to a bottom of the lowest subband.

Since mixing of the vertical modes and an appearance of additional lateral energy minima in magnetosubbands depend on $\Delta E_{21}^{(z)}$, we have repeated calculations for its smaller value. The left column in Fig.5 display the energy spectra for $\Delta E_{21}^{(z)} = 2$ meV and $\alpha = 0$. Again, in the absence of an in-plane magnetic field component ($B_y = 0$), subbands have parabolic shape but with lower energy spacings between neighbours. Now however, in contrary to the previous case, a moderate in-plane magnetic field ($B_y = 5$T) effectively mixes the vertical eigenmodes what leads to a formation of two equally deep minima for $\alpha = 0$ and one deep (the left one) and one shallow (the right one) for $\alpha = 0.02$. Note also that the subbands with negative energy dispersion relation which are lying higher on energy scale, cross with subbands of parabolic shape. These parabolic branches are formed when an electron occupies first excited state in vertical direction [in Eq.3 value of m is then reduced to m $= M = 2$]. These subbands are not mixed by magnetic field and have therefore different parity than those which were already mixed. These energy crossings survive also for $\alpha = 0.02$ [cf. Figs.5(d) and 5(f)]. Let us notice here, that such crossings are absent in the low energy spectra presented in Fig.4(c) due to the larger value of $\Delta E_{21}^{(z)}$ as well as due to a limited range of the energy scale in Figs. 4(e) and 4(f). For stronger magnetic field ($B_y = 10$ T) the energy minima for $\alpha = 0$ become more than five times deeper than for moderate field and almost two times deeper than those for $\Delta E_{21}^{(z)} = 5$ meV [cf. Figs. 5(e) and 4(e)].

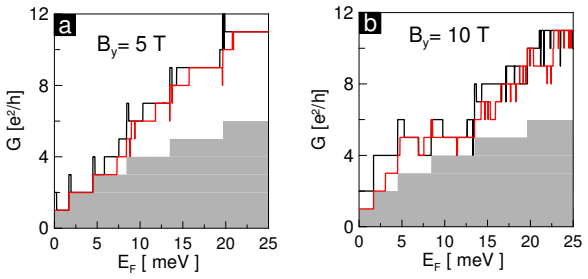

FIG. 6: (Color online) Spin-up conductance of a nanowire for a) $B_y = 5$ T, b) $B_y = 10$ T and $B_z = 0$. Results were obtained for a single layer wire [$M = 1$, grey region] and for a bilayer wire [$M = 2$, black and red colors]. Black colour marks conductance for $\alpha = 0$ ($\Delta E_{21}^{(z)} = 5$ meV) while red for $\alpha = 0.02$ ($\Delta E_{21}^{(z)} = 5.88$ meV).

In Fig.6 we have plotted the conductance of a bi-layer wire for spin-up electrons and that of a single-layer wire for comparison. Conductance has been calculated for temperature $T = 0$ by counting the crossings between the horizontal line at Fermi energy level with those parts of subbands which have $k_{kin} > 0$. Results obtained for a single-layer wire [$M = 1$] show standard, well-known step-like raising function (grey colour) with hights of steps equal to the conductance unit $G_0 = e^2/h$ [the spin degeneracy is lifted]. On the other hand, the conductance for a bi-layer wire [$M = 2$, red colour stands for $\alpha = 0$ while the black for $\alpha = 0.02$] still exhibits a step-like character but now two additional features appear: i) the heights of the steps may be equal to G_0 or $2G_0$ and, ii) the value of conductance drops by G_0 when the Fermi energy exceeds the height of the central maximum in a

particular subband. Due to a stronger coupling of the vertical modes for $B_y = 10$ T, the rising and the falling steps become better separated than for $B_y = 5$T. This is easily noticeable if we compare e.g. the changes in conductance for $E_F < 10$ meV in Figs.6 (a) and (b). When a confining potential looses spatial symmetry ($\alpha = 0.02$), the conductance of bi-layer nanosystem is generally lower than for $\alpha = 0$ and approaches in some points a lower limit established by the value of conductance of a single-layer wire. In both cases, even though the conductance is significantly larger for bi-layer wire than for a single-layer case, their ratio very rarely reaches its upper limit which equals 2.

C. Mixing of the vertical and the transverse modes in tilted magnetic field

If we account the vertical component of magnetic field ($B_z > 0$) in our considerations, then the term $Y^{(2)}_{i,j}$ appearing in the diagonal part of effective Hamiltonian [Eq.6] becomes responsible for mixing of the transverse eigenstates $\varphi_i(y)$ while the transverse and vertical eigenmodes can be simultaneously mixed by matrix elements H^{eff}_3 defined in Eq.10 if $\omega_y\omega_z \neq 0$. The latter term contribute to the off-diagonal elements in Eq.11 for $\alpha = 0$ due to non-zero value of $Z^{(1)}_{1,2}$ or simultaneously to the diagonal and off-diagonal submatrices in Eq.11 for $\alpha > 0$.

Magnetosubbands for $\Delta E^{(z)}_{21} = 2$meV and $B_z = 1$ T are plotted in Figs.7(a-c) for $\alpha = 0$ and in Fig.7(d) for $\alpha = 0.02$. For $B_y = 0$, subbands have parabolic-like shapes and do not cross each other. Since $\omega_y = 0$, all the off-diagonal elements [see Eqs.8-10] in effective Hamiltonian [Eq.11] vanish and only the diagonal elements given by Eq.7 survive but they cannot mix the vertical modes. Therefore, the subbands corresponding to vertical excitation of an electron [dashed lines in Fig.7(a)] are simply the replicas of those subbands in which the electron occupies the ground state in vertical direction. They are only shifted upwards on energy scale by $\Delta E^{(z)}_{21}$. The wave functions of these subbands have different symmetries with respect to reflection $z \to -z$ and for this reason may mutually intersect in higher part of energy spectrum for $B_y = 0$ [not shown in Fig.7(a)]. If both B_y and B_z have non-zero values, the off-diagonal elements in effective Hamiltonian which are defined by Eq.10 may mix the vertical and transverse modes since the products of terms $Y^{(1)}_{i,j}$ and $Z^{(1)}_{l,m}$ have non-zero values. In Fig.7(b) we see that for $B_y = 5$ T there are two deep lateral minima in the lowest subband similarily as in the case for $B_y > 0$ and $B_z = 0$ [cf. Figs. 4(c) and 5(c)]. However, for $B_z = 1$T, due to mixing of the transverse modes, the subbands lying higher on energy scale are not the replicas of the lowest one any longer. In vicinty of $k = 0$, crossings are replaced by avoided crossings at positions where they maximally mix with their neighbours what in consequence opens additional pseudogaps in the energy spectrum. The widths of antycrossings are dependent on B_y strength. If value of B_y is increased, then the spatial localizations of subbands in the lower and upper layers are enhanced. It diminishes the overlaps between transverse modes belonging to different layers what in consequence decreases the widths of anticrossings [cf. Figs. 7(b) and 7(c)]. Generally, the pattern of these avoiding crossings does not change much when th upper and lower quantum wells are slightly different [$\alpha = 0.02$] besides an accuracy of additional positive slope in energy [cf. Figs. 7(c) and 7(d)]. Even though, for $B_y = 5$ T the vertical modes shall be effectively mixed, the two deep lateral minima are present only in two lowest subbands. In upper subbands they are replaced by bending points due to a comparable mixing of the vertical and transverse modes. However, when the transverse component of magnetic field becomes two times stronger ($B_y = 10$ T), the coupling of vertical modes dominates in the system and these minima are again visible in the lowest subbands [cf. Figs. 7(c) and 7(d)]. In addition, the minima in question are localized at points $\pm k_m$ that is exactly as in the lowest subband [Fig.7(c)].

An appearance of additional pseudogaps in energy spectrum significantly modifies the conductane of a bi-layer wire. An example dependence of wire's conduc-

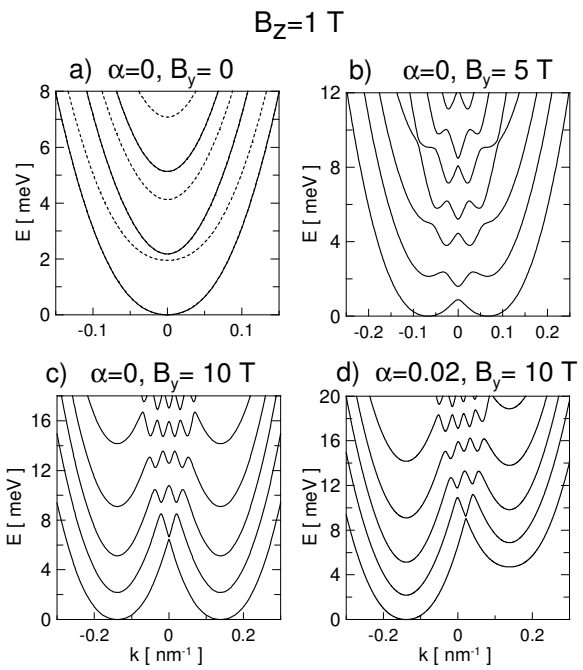

FIG. 7: Energy dispersion relation for $\Delta E^{(z)}_{21} = 2$ meV and $B_z = 1$ T for different values of B_y. Figures (a-c) show the results for $\alpha = 0$ while figure (d) for $\alpha = 0.02$. In (a) solid lines mark these subbands in which an electron occupies the ground state in growth direction [$f_1(z)$] while the dashed ones stand for the first exicited state [$f_2(z)$]. All energies are given with respect to a bottom of the lowest subband.

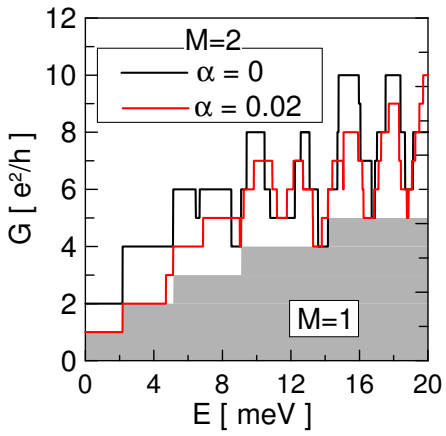

FIG. 8: (Color online) Spin-up conductance of a single layer ($M = 1$) and bi-layer wire ($M = 2$) calculated for $B_y = 10$ T and $B_z = 1$ T.

tance on Fermi energy is shown in Fig.8 for $B_z = 1$ T and $B_y = 10$ T. For symmetric confinement ($\alpha = 0$) the conductance raises by $2G_0$ when the energy exceeds the bottoms of the first three subbands [i.e. for $E = 0$ meV, $E = 2.18$ meV and $E = 5.13$ meV in Fig.8] which are determined by their lateral energy minima and it drops by G_0 for an energy exceeding next the central maximum in particular subband. When the energy is increased and passes through the pseudogap and then through the local energy minima localized in vicinity of $k = 0$, the value of conductance again jumps. Now however, the heights of G steps depend on the number of local minima belonging to a particular subband which equals the subband's index plus one. For example, in Fig.8 we see that the conductance grows by $4G_0$ when energy increases from 9.1 meV to 9.4 meV and even by $6G_0$ when it is changed between 14.2 meV and 14.8 meV. On the other hand, it may also significantly drop if an electron's energy is shifted through the set of local maxima localized in proximity of $k = 0$ because it enters a pseudogap region then. We notice such a large drop, being equal to $5G_0$, when Fermi energy is increased from 15.95 meV to 16.7 meV. Generally, the conductance steps for $\alpha = 0.02$ are lower than for $\alpha = 0$ mainly due to a considerable shift of energy levels ladder in the narrower layer. This effectively suppresses the mixing of vertical modes because the value of $\Delta E_{21}^{(z)}$ significantly grows then. The conductance of a single layer wire constitutes a lower bound for conductance of bi-layer wire. Both can be equal only if Fermi energy is localized within a pseudogap. Such case is visible in Fig.8 for both values of α and energies: 13.6 meV and 16.7 meV.

IV. SPIN POLARIZATION OF CONDUCTANCE IN BI-LAYER NANOWIRE

In previous sections we have discussed the process of formation of pseudogaps in electron's energy spectra and its influence on the wire's conductance but have neglected the spin Zeeman effect contribution to energy. An interaction of electron's spin with strong magnetic field, what is the case considered here, splits the spin-down and spin-up subbands by $\Delta E_Z = g\mu_B B$. For this reason, the conductance of bi-layer wire may be partly spin polarized[21] i.e. $\eta = (G_\uparrow - G_\downarrow)/(G_\uparrow + G_\downarrow) > 0$ and this polarization shall be dependent not only on a number of active spin-up and spin-down subbands as it is in the case of a single-layer wire but also on that whether the Fermi energy is pinned within the pseudogap or not. In the later case one may expect a larger value of η. In Fig.9 we have plotted the conductance, its derivative with respect to energy (dG/dE) and value of spin polarization of conductance (η) for bi-layer wire in function of B_y and energy for $B_z = 1$ T and $T = 0$ K. These outcomes were obtained for the wire made of GaAs [first and second columns for $\Delta E_{21}^{(z)} = 2.0,\ 5.0$ meV and $g = -0.44$] and of InGaAs[22] [third column for $\Delta E_{21}^{(z)} = 5$ meV and $g = -4.0$].

In three figures 9(a,d,g) which show the conductance, we may notice two characteristic regions lying above and under the anti-diagonal. In first region (above the anti-diagonal), the changes of conductance values are frequent and can be increased as well as decreased when electron's energy grows. The second characteristic region appears rather for strong magnetc field (under anti-diagonal). It has more regular pattern resembling very much that of a single layer quantum wire as the value of conductance increases by G_0 when subsequent subband becomes active. Besides the conductance, also a transconductance is very often measured in experiment as it directly reveals the dynamical properties of nanosystem being sensitive to the variations of voltages applied to metallic gates[23] used e.g. to tune the Fermi energy in the wire. Figures 9(b,e,h) show dependence of similar quantity i.e. dG/dE on B_y and energy values. For GaAs, that has low value of g factor, subsequent spin-up and spin-down subbands are gathered in pairs even for strong B_y due to a small energy splitting [Figs.9(b),(e)]. However, because of small Zeeman energy splitting, conductance becomes partly polarized only for a very narrow energy stripes what show Figs.9(c) and 9(f). Despite this fact, we have found that even for GaAs wire, conductance can to a large extent be spin polarized. For example, for $\Delta E_{21}^{(z)} = 2$meV [Fig.9(c)] polarization may reach 60% and 50% for pairs of parameters: $B_y = 5.94$ T, $E = 3.54$ meV and $B_y = 6.69$ T, $E = 6.63$ meV, respectively. Regions with similar values of polarization we have also found in Fig.9(f) for $\Delta E_{21}^{(z)} = 5$ meV.
If a bi-layer nanowire is made of InGaAs which has much larger g factor than GaAs, then an energy splitting due to

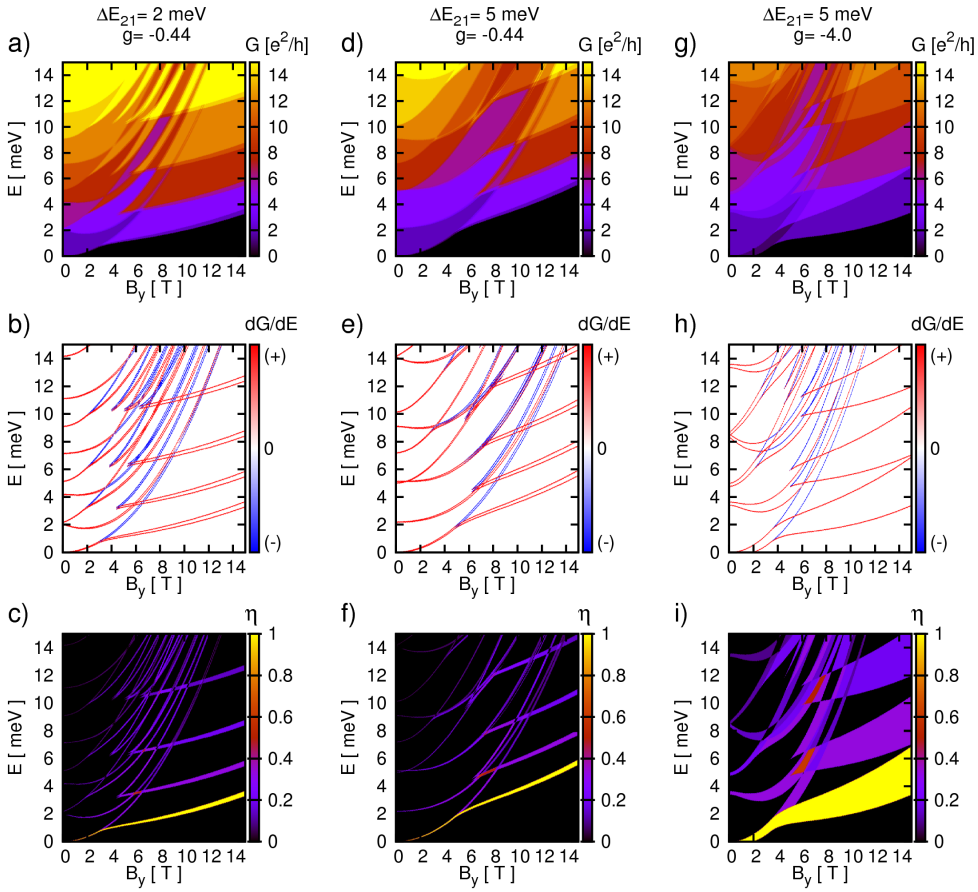

FIG. 9: (Color online) Conductance (1-st row), its derivative dG/dE (2-nd row) and spin polarization of conductance (3-rd row) for bi-layer quantum wire. First and second columns presents the results for GaAs while third column for InGaAs. The energy difference $\Delta E_{21}^{(z)}$ is displayed on top of each columns. Value of vertical component of magnetic field equals $B_z = 1$ T. All energies are shifted down so as to the lowest subband has zero energy for $B_y = 0$. Therefore, in order to get the Fermi energy, an energy of the lowest subband must be subtracted before.

spin Zeeman effect becomes even comparible with an energy difference between the bottoms of two neighbouring subbands [see the right part of Fig.9(h)]. In such case, subbands with negative energy dispersion relation (blue curves) are shifted significantly on energy scale even for moderate magnetic field [e.g. $B_y \approx 4 - 8$ T in Fig.9(h)]. For this reason, the regions of partly spin polarized conductance appearing for a wire with low g factor in form of narrow stripes, now become much wider [see two distinct reddish stripes appearing near the central part of Fig.9(i), which mark 60% and 50% conductance polarization, respectively]. This example show the advantage of bilayer quantum wire over e.g. Y-shaped nanostructures[24,25] in preparing partially spin polarized current. Bi-layer nanowire enables one to get partially spin polarized current not only for the lowest subband but also for those lying higher on energy scale giving thus larger conductances and currents. Drawback of this solution is however that, it still requires a strong magnetic field to work.

We have repeated calculations for spin polarization of conductance for InGaAs wire for temperature $T = 4.2$ K. Results are displayed in Fig.10. As expected, the temperature smearing of subbands makes the originally moderately spin polarized regions smaller and additionally, it lowers their polarization to about 30%. This unvafourable effect can however be limited if semiconductor materials with much larger g factor like e.g. InSb[26] or InAs[27] are to be used for the nanowire fabrication process.

V. CONCLUSIONS

We have theoretically investigated an effect of the magnetic field on the inter-layer and intra-layer subbands mixing for two vertically aligned nanowires with a rectangular-like external confining potential. For this purpose, a simple semi-analytical method was developed which has enabled us to calculate the energy subbands in dependence on electron's wave vector value. It has

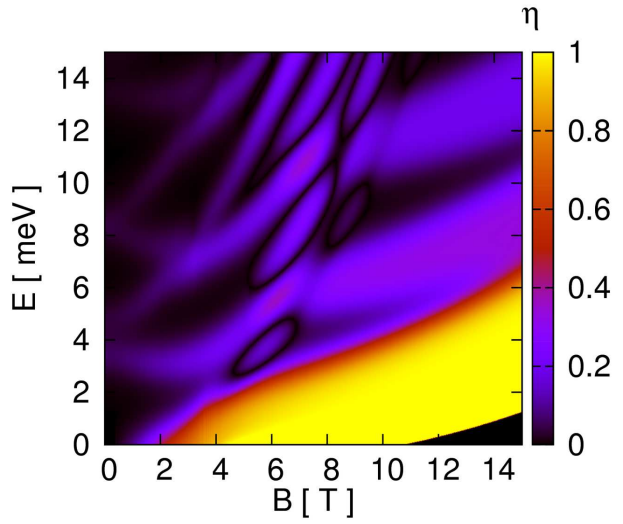

FIG. 10: (Color online) Spin polarization of conductance for InGaAs bi-layer quantum wire for T = 4.2 K. Other parameters are the same as for Fig.9(i): $g = -4.0$ and $\Delta E_{21}^{(z)} = 5$ meV.

been showed, that the transverse component of magnetic field, which is perpendicular to the wire's axis but parallel to the layers, can effectively mix two lowest vertical eigenmodes what transforms the low energy subbands' parabolas into slowly oscillating curves with two deep lateral energy minima. If besides the transverse component of magnetic field, the vertical one is also taken into account, then both the vertical and transverse modes are mixed simultaneously, crossings between subbands are replaced by avoided crossings what lifts the degeneracy between subbands in vicinity of $k = 0$ and additional small pseudogaps appear in the energy spectrum. A qualitatively similar behaviour of magnetosubbands were predicted for two laterally aligned wires by Shi and Gu.[9] They showed that only one component of magnetic field, namely the perpendicular one, is needed for an effective mixing of all pairs of magnetosubbands which were originally localized in the same and in different wires. Consequently, such unrestricted hybridization of magnetosubbands gives then simultaneously both types of oscillations in energy spectrum E(k) that is, two deep lateral minima and the small-amplitude oscillations near $k = 0$. In contrary to a nanosystem with two laterally aligned wires, an interlayer subbands hybridization in the vertically aligned bi-layer wire depends on the transverse component of magnetic field only while the perpendicular one is responsible for the intralayer modes mixing.

Irrespective of the coupling direction, if these small-amplitude oscillations appear in energy dispersion relation E(k) then the conductance of a bi-layer wire may jump as well as drop by a few conductance quanta provided that the confining potential has low number of defects. When Fermi energy is shifted through these oscillations, value of conductance first jumps and then falls, within a thin energy region, even by several units of conductance. Results of our simulations show that the conductance of bi-layer quantum wire can be spin-polarized up to 60% at zero temperature. Magnitude of spin polarization can be tuned by changing the strength of magnetic field and the value of Fermi energy.

Although there are no direct experimental results confirming our predictions, a number of experiments were performed for similar bi-layer nanosystems. Thomas et al.[8] have measured the conductance of two vertically coupled wires in dependence of the top gate voltages for parallel and perpendicular magnetic fields. Also in work of Fischer et al.[7], the conductance of similar bi-layer nanowire with nonsymmetric vertical confining potential was experimentally investigated. In both experiments however, the lateral confinement was smooth whereas our predictions concern the nanowires with rectangular-like lateral confinement and therefore the outcomes of calculations and the experimental data can not be directly compared.

Acknowledgements

The work was financed by Polish Ministry of Science and Higher Education (MNiSW)

References

* Electronic address: chwiej@fis.agh.edu.pl

[1] C. C. Eugster and J. A. del Alamo, Phys. Rev. Lett. **67**, 3586 (1991).
[2] O. Bierwagen, C. Walther, W. T. Masselink, and K.-J. Friedland, Phys. Rev. B **67**, 195331 (2003).
[3] S. K. Lyo, J. Phys.: Condens. Matter **8**, L703 (1996).
[4] L. G. Mourokh, A. Y. Smirnov, and S. F. Fischer, Appl. Phys. Lett. **90**, 132108 (2007).
[5] S. F. Fischer, G. Apetrii, U. Kunze, D. Schuh, and G. Abstreiter, Phys. Rev. B **74**, 115324 (2006).
[6] D. Huang, S. K. Lyo, K. J. Thomas, and M. Pepper, Phys. Rev. B **77**, 085320 (2008).
[7] S. F. Fischer, G. Apetrii, U. Kunze, D. Schuh, and G. Abstreiter, Phys. Rev. B **71**, 195330 (2005).
[8] K. J. Thomas, J. T. Nicholls, M. Y. Simmons, W. R. Tribe, A. G. Davies, and M. Pepper, Phys. Rev. B **59**, 12252 (1999).
[9] J.-R. Shi and B.-Y. Gu, Phys. Rev. B **55**, 9941 (1997).
[10] E. Bielejec, J. A. Seamons, J. L. Reno, and M. P. Lilly, App. Phys. Lett. **86**, 083101 (2005).
[11] S. Kumar, K. J. Thomas, L. W. Smith, M. Pepper, G. L. Creeth, I. Farrer, D. Ritchie, G. Jones, and J. Griffiths,

Phys. Rev. B **90**, 201304 (2014).
[12] S. Buchholz, S. Fischer, U. Kunze, D. Schuh, and G. Abstreiter, Physica E **40**, 1448 (2008).
[13] W. K. Hew, K. J. Thomas, M. Pepper, I. Farrer, D. Anderson, G. A. C. Jones, and D. A. Ritchie, Phys. Rev. Lett. **102**, 056804 (2009).
[14] Fischer S. F., Apetrii G., Kunze U., Schuh D., and Abstreiter G., Nat. Phys. **2**, 91 (2006).
[15] A. Tarasov, S. Hugger, H. Xu, M. Cerchez, T. Heinzel, I. V. Zozoulenko, U. Gasser-Szerer, D. Reuter, and A. D. Wieck, Phys. Rev. Lett. **104**, 186801 (2010).
[16] M. Huber, M. Grayson, M. Rother, W. Biberacher, W. Wegscheider, and G. Abstreiter, Phys. Rev. Lett. **94**, 016805 (2005).
[17] N. R. Abdullah, C.-S. Tang, and V. Gudmundsson, Phys. Rev. B **82**, 195325 (2010).
[18] S. Ihnatsenka and I. V. Zozoulenko, Phys. Rev. B **73**, 075331 (2006).
[19] S. Schnez, C. Rössler, T. Ihn, K. Ensslin, C. Reichl, and W. Wegscheider, Phys. Rev. B **84**, 195322 (2011).
[20] B. Hackens, F. Delfosse, S. Faniel, C. Gustin, H. Boutry, X. Wallart, S. Bollaert, A. Cappy, and V. Bayot, Phys. Rev. B **66**, 241305 (2002).
[21] P. P. Das, N. K. Bhandari, J. Wan, J. Charles, M. Cahay, K. B. Chetry, R. S. Newrock, and S. T. Herbert, Nanotechnology **23**, 215201 (2012).
[22] A. V. Ramos, M.-J. Guittet, J.-B. Moussy, R. Mattana, C. Deranlot, F. Petroff, and C. Gatel, App. Phys. Lett. **91**, 122107 (2007).
[23] S. F. Fischer, G. Apetrii, U. Kunze, D. Schuh, and G. Abstreiter, Phys. Rev. B **74**, 115324 (2006).
[24] A. W. Cummings, R. Akis, D. K. Ferry, J. Jacob, T. Matsuyama, U. Merkt, and G. Meier, J. Appl. Phys. **104**, 066106 (2008).
[25] P. Wócik, J. Adamowski, M. Wołoszyn, and B. J. Spisak, J. Appl. Phys. **118**, 014302 (2015).
[26] S. Nadj-Perge, V. S. Pribiag, J. W. G. van den Berg, K. Zuo, S. R. Plissard, E. P. A. M. Bakkers, S. M. Frolov, and L. P. Kouwenhoven, Phys. Rev. Lett. **108**, 166801 (2012).
[27] S. Nadj-Perge, S. M. Frolov, J. W. W. van Tilburg, J. Danon, Y. V. Nazarov, R. Algra, E. P. A. M. Bakkers, and L. P. Kouwenhoven, Phys. Rev. B **81**, 201305 (2010).